How to cite: *Angew. Chem. Int. Ed.* **2021**, *60*, 268 – 273
International Edition: doi.org/10.1002/anie.202011765
German Edition: doi.org/10.1002/ange.202011765

Thermoelectricity Hot Paper

Strong Valence Band Convergence to Enhance Thermoelectric Performance in PbSe with Two Chemically Independent Controls

Zhong-Zhen Luo, Songting Cai, Shiqiang Hao, Trevor P. Bailey, Ioannis Spanopoulos, Yubo Luo, Jianwei Xu, Ctirad Uher, Christopher Wolverton, Vinayak P. Dravid, Qingyu Yan, and Mercouri G. Kanatzidis**

Abstract: *We present an effective approach to favorably modify the electronic structure of PbSe using Ag doping coupled with SrSe or BaSe alloying. The Ag 4d states make a contribution to in the top of the heavy hole valence band and raise its energy. The Sr and Ba atoms diminish the contribution of Pb $6s^2$ states and decrease the energy of the light hole valence band. This electronic structure modification increases the density-of-states effective mass, and strongly enhances the thermoelectric performance. Moreover, the Ag-rich nanoscale precipitates, discordant Ag atoms, and Pb/Sr, Pb/Ba point defects in the PbSe matrix work together to reduce the lattice thermal conductivity, resulting a record high average ZT_{avg} of around 0.86 over 400–923 K.*

Introduction

With about two-thirds of the world's produced energy being lost as waste heat,[1] thermoelectric materials which are capable of converting waste heat directly into electricity and have received worldwide research attention. The conversion efficiency of a thermoelectric material is governed by the dimensionless figure of merit, $ZT = S^2\sigma T/(\kappa_{car} + \kappa_{lat})$, where S, σ, T, κ_{car} and κ_{lat} are the Seebeck coefficient, electrical conductivity, absolute temperature in Kelvin, and carrier and lattice thermal conductivities, respectively.[2] It is apparent that high ZT can be obtained through enhanced power factor ($PF = S^2\sigma$) or decreased κ_{tot} ($\kappa_{car} + \kappa_{lat}$) or both. The strong coupling between S, σ, and κ_{car} makes it is very difficult to enhance ZT. The efficiency of a thermoelectric device ($\eta = [(T_H - T_C)/T_H]\ [(1 + ZT_{avg})^{1/2} - 1]/[(1 + ZT_{avg})^{1/2} + T_C/T_H]$, where T_H and T_C are the hot-side and cold-side temperature, respectively) is directly dependent on the magnitude of the average ZT over the entire temperature range of operation, which is historically challenging to enhance.[3] Therefore, for efficient heat to electrical energy conversion, it is not sufficient to just increase the maximum value of ZT if the average ZT_{avg} over a broad temperature range remains low.

PbTe is one of the best thermoelectric materials for power generation because of its unique electronic band structure (two valence bands: the light (L) and the heavy (Σ) valence band) and intrinsically low thermal conductivity.[4] However, elemental Te is rare and expensive, which motivates a search for high-performing Te-free compounds. In this context, PbSe is supposed to be one of the most promising candidates because selenium is about fifty times more earth abundant than tellurium and this has sparked much interest in the thermoelectrics community.[5] Although PbSe has a similar electronic structure with two valence bands structure, the thermoelectric performance of p-type PbSe is quite inferior to p-type PbTe. This is primarily caused by the much larger energy difference ΔE_v (0.28 eV) than PbTe (0.15 eV), which inhibits the full contribution of the heavy (Σ) valence band to charge transport at the temperatures of interest (600–1000 K). With the weak influence from the second valence band Σ, PbSe exhibits lower Seebeck coefficient and PbSe can be regarded essentially as a single-valence-band semiconductor below 600 K.[5h,6] As one of the most important strategies for improving thermoelectric performance, band convergence has virtually no detrimental effects.[7] However, in lead chalcogenides, the alkali metals Na and K serve only as ideal dopants to optimize the carrier concentration and do not modify the electronic band structure.[5b,8] On the other hand, although n-type PbSe has approximate maximum $ZT \approx 1.6$, the excellent ZT_{avg} of ≈ 1.1 over 400–923 K for n-type PbSe has been achieved via the alloying of so-called discordant Ge atoms, which strongly reduce the lattice thermal conductivity.[9] In contrast, the corresponding p-type ZT_{avg} value is only ≈ 0.6.[5a] Thus, the simultaneous reduction of ΔE_v achieved by light and the heavy valence band convergence and κ_{lat} is essential to improving the performance of p-type PbSe, and in particular the ZT_{avg}.

[*] Dr. Z.-Z. Luo, Dr. Y. Luo, Prof. Q. Yan
School of Materials Science and Engineering, Nanyang Technological University
50 Nanyang Avenue, Singapore 639798 (Singapore)
E-mail: alexyan@ntu.edu.sg
Dr. Z.-Z. Luo, S. Cai, Dr. I. Spanopoulos, Dr. Y. Luo, Prof. M. G. Kanatzidis
Department of Chemistry, Northwestern University
Evanston, Illinois 60208 (USA)
E-mail: m-kanatzidis@northwestern.edu
S. Cai, Dr. S. Hao, Prof. C. Wolverton, Prof. V. P. Dravid
Department of Materials Science and Engineering, Northwestern University
Evanston, Illinois 60208 (USA)
Dr. T. P. Bailey, Prof. C. Uher
Department of Physics, University of Michigan
Ann Arbor, Michigan 48109 (USA)
Prof. J. Xu
Institute of Materials Research and Engineering, A*STAR (Agency for Science, Technology and Research)
2 Fusionopolis Way, Innovis #08-03, Singapore 138634 (Singapore)
Supporting information and the ORCID identification number(s) for the author(s) of this article can be found under: https://doi.org/10.1002/anie.202011765.

In this study, we find Ag dopant does not only optimize the carrier concentration but also markedly reduces the valence band offset energy, ΔE_v, which can then be further decreased by the second agent SrSe or BaSe alloying. This causes a much decreased ΔE_v that moves the onset of the valence band convergence to lower temperatures ($\approx$450 K) than by using just SrSe or BaSe alone.[5b,10] We refer to this effect as dual chemical knob control of the valence band converge, which induces a superior rise of the Seebeck coefficient with temperature beginning above $\approx$450 K, compared to the corresponding Na-doped PbSe-SrSe/BaSe samples.[5b,11] This is the first time that a metallic dopant has been discovered to affect the orbital constitution of the top of the heavy hole valence band. Moreover, because its concentration is the beyond the solubility limit in the PbSe matrix, Ag-rich nanoscale precipitates are formed. This is in addition to the discordant Ag atoms in the lattice and the Pb/Sr, Pb/Ba point defects, all of which work together to cause intense phonon scattering and reduce the lattice thermal conductivity to $\approx$0.60 $Wm^{-1}K^{-1}$ at 823 K. As a result, the ZT values are increased at all temperatures producing a record high ZT_{avg} of 0.86 at 400–923 K in $Pb_{0.99}Ag_{0.01}Se$-1.5 % SrSe.

Results and Discussion

The powder X-ray diffraction (PXRD) patterns of all $Pb_{0.99}Ag_{0.01}Se$-x%SrSe and $Pb_{0.99}Ag_{0.01}Se$-y%BaSe samples (see Figure S1 in Supporting Information) indicate apparent single-phase compounds with a NaCl type structure. To get a deeper understanding of Ag-doping and Sr alloying on the microstructure of PbSe, we performed scanning/transmission electron microscopy (S/TEM) analyses. As shown in Figure S3a, the high-angle annular dark field (HAADF) image of $Pb_{0.995}Ag_{0.005}Se$ shows a clean surface without any z-contrast observable. Along with the corresponding energy dispersive spectroscopy (EDS) mappings, it is confirmed that the 0.5 % Ag are all doped into the PbSe matrix. When the Ag concentration is increased to 1 %, most of the specimen is still a solid solution but a very sparse amount of Ag-rich second phases (highlighted by yellow arrows) is also present, see Figure S3b. However, when the SrSe fraction is further raised to 1.5 %, the solubility of Ag in PbSe decreases dramatically. As highlighted by yellow arrows in Figure 1a and c, a large amount of nanoscale precipitates are observed to be homogeneously distributed in the matrix. The precipitates are rich in Ag according to EDS mapping, with a size range of 5–80 nm (Figure 1b). The selected area diffraction pattern (inset of Figure 1c) matches the rock-salt cubic PbSe along the [110] zone axis, with no extra spot observable. The high-resolution TEM image of nanoprecipitates embedded in the matrix reveals a coherent boundary between the Ag-rich phase and its surroundings (Figure 1d).

As shown in the calculated projected density of states (Figures 2b,d and f), the conduction band minimum stems mainly from Pb 6p states, while the valence L band maxima come from Se 4p, Ag 4d and Pb 6s states for Ag-doped and SrSe- or BaSe-alloyed PbSe. Compared with the band structure of pure PbSe, SrSe- or BaSe-alloyed PbSe systems

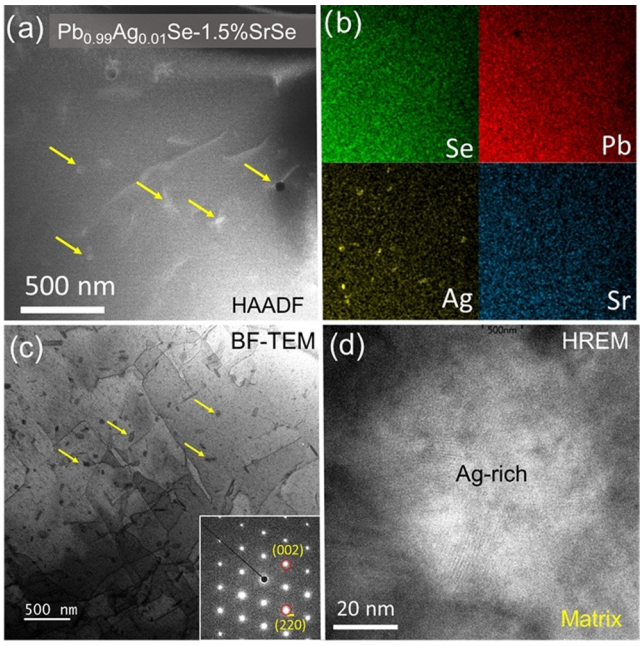

Figure 1. S/TEM analyses of $Pb_{0.99}Ag_{0.01}Se$-1.5 %SrSe sample. a) High-angle annular dark field (HAADF) image and b) corresponding EDS mappings. A decent amount of Ag-rich nanoscale precipitates are observable and are highlighted by the yellow arrows. c) Conventional bright field TEM image. Inset is the selected area diffraction pattern taken along the [110] zone axis of the PbSe matrix. d) High-resolution TEM image of one typical precipitate embedded in the matrix, revealing a coherent interface with its surroundings.

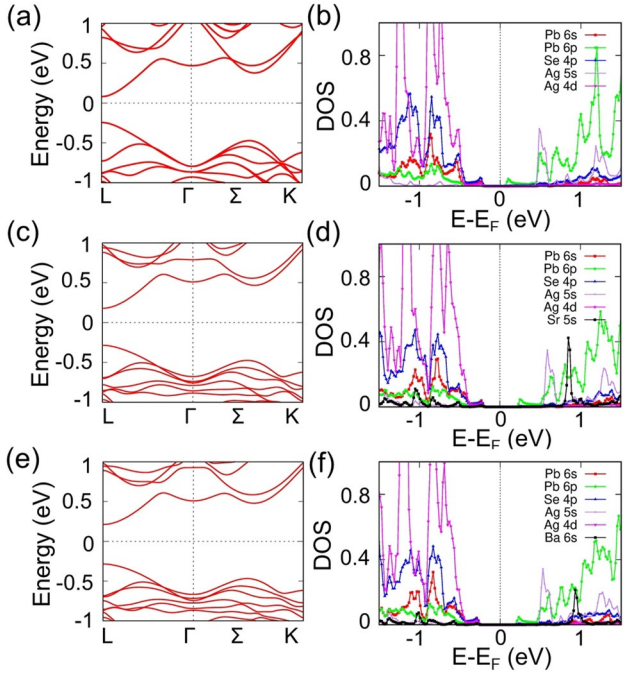

Figure 2. Electronic band structures of Ag-doped PbSe with $\Delta E_v \approx 0.21$ eV (a); Ag-doped and SrSe-alloyed PbSe with $\Delta E_v \approx 0.17$ eV (c); Ag-doped and BaSe-alloyed PbSe with $\Delta E_v \approx 0.17$ eV (e); and corresponding density of states for Ag-doped PbSe (b); Ag-doped and SrSe-alloyed PbSe (d); Ag-doped and BaSe-alloyed PbSe (f), where the corresponding states with only one atom in each species are displayed to clearly show their contribution.

(Figure S6), the Ag 4d state not only makes a contribution to L band, but also is the major component in heavy valence band (along Σ) for Ag-doped PbSe systems (Figure 2, Figures S7 and S8). As shown in Figures 2 a,c,e and S5, the energy offset, ΔE_v between the first valence band maximum (L point) and the second valence band maximum (along Σ) decreases for Ag-doped PbSe alloyed with SrSe or BaSe. Specifically, for the Ag-doped and SrSe- or BaSe-alloyed system, the energy offset reduces to only 0.17 eV, which is much smaller than the pure PbSe case of 0.28 eV.

To better clarify the role of SrSe and BaSe on this band convergence effect, we calculated the electronic band structures of the PbSe-SrSe and PbSe-BaSe alloys without any Ag added, see Figures S6b, S6c, S6e and S6f. As can be seen, the valence band maximum (VBM) band energy offsets are 0.21 and 0.20 eV caused by partially remove the weight of Pb $6s^2$ lone pair electrons on L,[12] which is the most approach of band convergence for the isoelectronic substituted PbQ-based materials.[5a,13] Interestingly, the energy offset is induced from the Se atoms around Sr or Ba atoms, while the Sr or Ba atoms themselves do not change the band structure appreciably.

A surprising revelation comes from studying the Ag effects on the electronic structure. To clearly show the contribution of Ag for the top VBMs, the valence band structures of Ag-doped and SrSe-alloyed PbSe is displayed in Figure 3 with the contribution of Pb 6s, Se 4p, Ag 4d and Sr 5s states from a single Pb, Se, Ag and Sr atoms. The bigger size of the dot the larger the contribution from the corresponding atom. As can be seen, for the first valence band maximum at L point, it is almost the same amount of contribution from Se 4p and Ag 4d states. However, for the second valence band maximum along the Σ direction, the contribution of the Ag 4d states is more significant about 3 times bigger than other orbital states from Se 4p and Pb 6s. This difference in orbital contribution can also be seen from the partial DOS from each single species in Figure 2 d, where at −0.45 eV (corresponding to the second VBM), the DOS value of Ag 4d state is much bigger than the Se 4p value. In addition, the first and second valence band carrier effective masses of Ag-doped PbSe increased to 0.12 m_0 and 1.96 m_0 from 0.11 m_0 and 1.90 m_0 for pure PbSe. Thus, the reduction of ΔE_v between the light and heavy valence bands due to the introduction of Ag can be understood by an increase of the energy of both the first and second VBM.

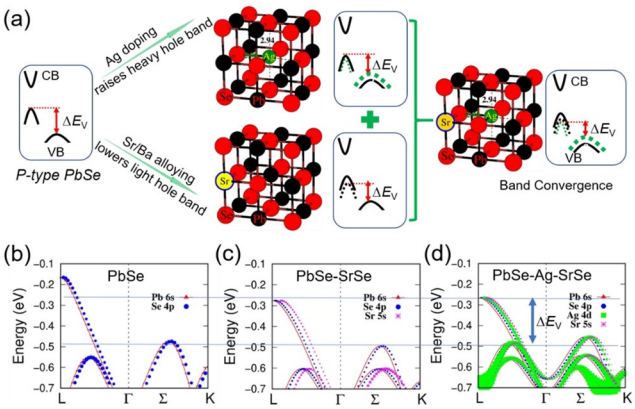

Figure 3. Figure Caption. a) The schematic of the band structure modification with Ag doping and SrSe/BaSe alloying as the two chemical independent controls. The Ag doping raises the heavy hole band and Sr/BaSe alloying lowers the light hole band, leading to the fast band convergence. This is the first time a significant modification has been discovered on the orbital constitution of the top of the heavy hole valence band by a dopant. The valence band structures of b) SrSe-alloyed (PbSe-SrSe) and c) Ag-doped and SrSe-alloyed PbSe (PbSe-Ag-SrSe) with the contribution of Pb 6s (red up triangle), Se 4p (blue circle), Sr 5s (pink star) and Ag 4d (green square) states from a single Pb, Se, Ag and Sr atoms. To highlight the contribution of Ag, all bands are shifted horizontally to make every species contribution visible.

It is well known that standard dopants (e.g. Na, K, Tl, etc.) can cause energy changes and modifications to the top of the light hole valence band (L point) in lead chalcogenides. However, these dopants leave the heavy whole band (Σ point) intact. The fact that a dopant can cause a significant modification on the constitution of the top of the heavy hole valence band is an important discovery because it points to a new chemical tuning method for this band. Therefore, the Ag-doping combined with SrSe- or BaSe-alloying achieves a larger effect in the reduction of ΔE_v than Ag alone or SrSe/BaSe alone. Furthermore, according to the calculation of lattice parameter as a function of temperature ($\alpha = \alpha_0 + \beta T + \gamma T^2$, where α_0 is 6.171, β is 5.55×10^{-5}, γ is 1.17×10^{-7}),[14] the lattice constant increases to 6.290 Å at 800 K without including the effects of dopants. Therefore, the energy offset decreases further to 0.14 eV for Ag-doped PbSe with SrSe alloyed system and 0.15 eV for Ag-doped PbSe with BaSe alloyed system, as shown in Figures S7 and S8.

These results are supported by temperature-dependent Hall coefficients (Figures S11a and S12a) and Photoemission Yield Spectroscopy in Air (PYSA) data (Figure S4). The occurrence of a maximum in the Hall coefficient T_H signifies the convergence temperature of the two valence bands.[10,15] For Ag-doped and SrSe alloyed sample, the T_H is ≈550 K, which is the lowest temperature reported in PbSe-based material systems,[5b,10,13b,15] indicating the smallest ΔE_V value obtained.[10] And from the PYSA measurement, ΔE_v is reduced from ≈0.25 for pure PbSe to ≈0.18 eV for both SrSe- and BaSe-alloyed samples at room temperature. As we will present below, this significant energy band convergence contributes to the significant enhancement of the Seebeck coefficients.

The temperature-dependent electrical conductivity of $Pb_{0.99}Ag_{0.01}Se$-x%SrSe and $Pb_{0.99}Ag_{0.01}Se$-y%BaSe samples decreases with increasing SrSe and BaSe fractions, Figures 4 a and 4b. This is in agreement with the simultaneous drops in n (Figure S10). At room temperature, the electrical conductivity of the SrSe-alloyed samples decreases from ≈2103 S cm^{-1} for $Pb_{0.99}Ag_{0.01}Se$ to ≈636 S cm^{-1} for $Pb_{0.99}Ag_{0.01}Se$-4%SrSe (Figure 4 a). For BaSe-alloyed samples, σ decreases to ≈665 S cm^{-1} for $Pb_{0.99}Ag_{0.01}Se$-5%BaSe (Figure 4 b). The electrical conductivity for both SrSe- and BaSe-alloyed sets of samples monotonously decreases with rising temperature, representing degenerate semiconductor behavior.

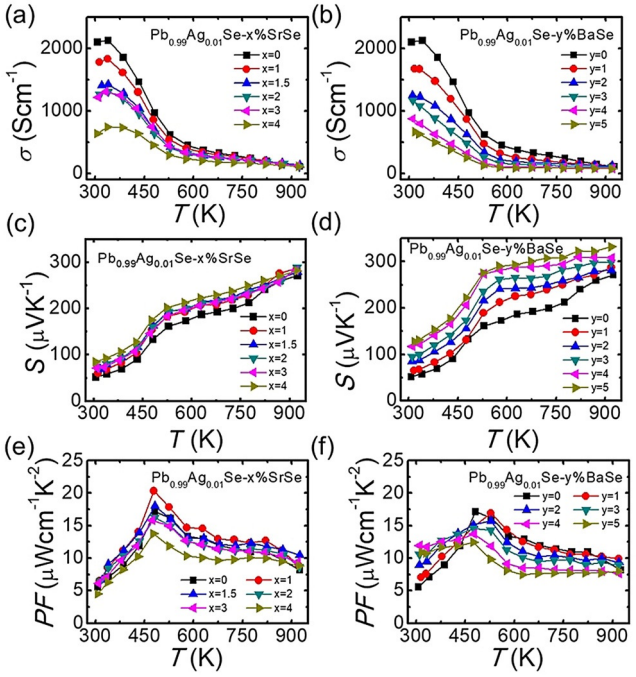

Figure 4. Thermoelectric properties as a function of temperature for $Pb_{0.99}Ag_{0.01}Se$-*x*%SrSe and $Pb_{0.99}Ag_{0.01}Se$-*y*%BaSe: electrical conductivity, σ (a) and (b); Seebeck coefficient, *S* (c) and (d); and power factor, *PF* (e) and (f).

The temperature-dependent Seebeck coefficients of $Pb_{0.99}Ag_{0.01}Se$-*x*%SrSe and $Pb_{0.99}Ag_{0.01}Se$-*y*%BaSe samples are shown in Figures 4c and d. The positive Seebeck coefficients throughout the tested temperature range confirm the p-type transport behavior suggested by the positive values of the Hall coefficients (Figure S10). At room temperature, the Seebeck coefficients of SrSe-alloyed samples gradually increase from $\approx 52\ \mu V K^{-1}$ for $Pb_{0.99}Ag_{0.01}Se$ to $\approx 84\ \mu V K^{-1}$ for $Pb_{0.99}Ag_{0.01}Se$-4% SrSe (Figure 4c). For BaSe-alloyed samples, the room-temperature Seebeck coefficients significantly increase to $\approx 128\ \mu V K^{-1}$ for $Pb_{0.99}Ag_{0.01}Se$-5% BaSe (Figure 4d). Moreover, the Seebeck coefficients are larger in samples with higher alloyed fraction in the entire measured temperature range. The coefficients for all samples increase with temperature and reach the maximum values of $\approx 288\ \mu V K^{-1}$ for $Pb_{0.99}Ag_{0.01}Se$-2% SrSe and $\approx 322\ \mu V K^{-1}$ for $Pb_{0.99}Ag_{0.01}Se$-5% BaSe at 923 K, respectively. Specifically, the Seebeck coefficients have a substantial increase beginning at ≈ 450 K, which is not observed for Na-doped PbSe-SrSe/BaSe samples (Figure S13).[5b,11,16] We attribute the lower onset temperature of this enhancement to the superior dual chemical knob valence bands convergence caused by the significantly decreased ΔE_v (Figures 2e and f, and Figure S5). Moreover, from the Pisarenko relation (Seebeck coefficients as a function of carrier concentration) as shown in Figure S16, the increased m^* derives from the strong L-Σ band convergence effect and results in the enhancement of the Seebeck coefficient.[13d] More importantly, the Seebeck coefficients are robust to annealing the samples (Figure S14) and also repeatable in multiple measurements (Figure S15).

The temperature-dependent power factors of $Pb_{0.99}Ag_{0.01}Se$-*x*%SrSe and $Pb_{0.99}Ag_{0.01}Se$-*y*%BaSe samples are displayed in Figures 4e and f. The room temperature power factors are above 5 $\mu W cm^{-1} K^{-2}$ for all samples, which is much higher than 1.63 $\mu W cm^{-1} K^{-2}$ for $Pb_{0.99}Na_{0.01}Se$-2% SrSe and 2.10 $\mu W cm^{-1} K^{-2}$ for $Pb_{0.99}Na_{0.01}Se$-3% BaSe (Figure S17).[11b] Moreover, the power factors rapidly increase at elevated temperature and reach $\approx 20\ \mu W cm^{-1} K^{-2}$ at 473 K for $Pb_{0.99}Ag_{0.01}Se$-1% SrSe (Figure 4e). For BaSe-alloyed samples, the highest value is $\approx 17\ \mu W cm^{-1} K^{-2}$ at 523 K for $Pb_{0.99}Ag_{0.01}Se$-1% BaSe (Figure 4f). Compared with the previous PbSe-based materials,[5a,11,13b,15] the Ag-doped and SrSe- or BaSe-alloyed samples exhibit much higher power factors at the range of 300–600 K, as shown in Figure S17. The superior power factors, especially at low temperature range (< 600 K) is a very important advantage for achieving the high ZT_{avg}.

The temperature-dependent κ_{tot} of $Pb_{0.99}Ag_{0.01}Se$-*x*%SrSe and $Pb_{0.99}Ag_{0.01}Se$-*y*%BaSe samples is displayed in Figures 5a and b. At room temperature, the κ_{tot} decreases with the increased SrSe or BaSe fraction, from 3.03 $W m^{-1} K^{-1}$ for $Pb_{0.99}Ag_{0.01}Se$ to 1.97 and 1.61 $W m^{-1} K^{-1}$ for $Pb_{0.99}Ag_{0.01}Se$-4% SrSe and $Pb_{0.99}Ag_{0.01}Se$-5% BaSe, respectively. Moreover, the κ_{tot} is lower with higher SrSe/BaSe alloy fraction in the measured temperature range. For all samples, the κ_{tot} continuously decreases with rising temperature and becomes 0.84 and 0.76 $W m^{-1} K^{-1}$ at 873 K for SrSe and BaSe-alloyed samples, respectively.

The κ_{lat} is calculated by the equation: $\kappa_{lat} = \kappa_{tot} - \kappa_{car} = \kappa_{tot} - L\sigma T$ (where *L* is the Lorenz number, evaluated by the equation: $L = (1.5 + \exp[-|S|/116]) \times 10^{-8}\ V^2 K^{-2}$).[17] The κ_{car} and calculated *L* are displayed in Figures S18c, S18d, S18e, and S18f. Both the SrSe and BaSe alloying can efficiently enhance the scattering of phonons by point defects mainly from the mass and strain fluctuations in the lattice, resulting in reduced κ_{lat} (Figures 5c and d). Moreover, the κ_{lat} decreases at the increasing temperature as usually occurs in semiconductors caused by phonon-phonon umklapp scattering. In detail, for SrSe-alloyed samples, the lowest κ_{lat} value of

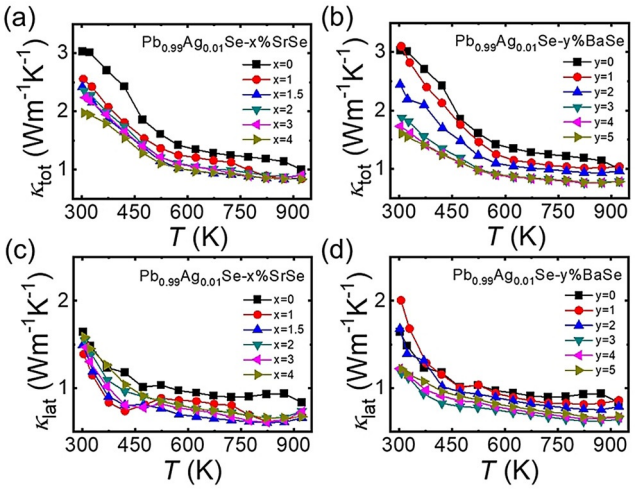

Figure 5. Thermal properties as a function of temperature for $Pb_{0.99}Ag_{0.01}Se$-*x*%SrSe and $Pb_{0.99}Ag_{0.01}Se$-*y*%BaSe: total thermal conductivity, κ_{tot} (a) and (b); and lattice thermal conductivity, κ_{lat} (c) and (d).

$\approx 0.60\ Wm^{-1}K^{-1}$ is obtained for $Pb_{0.99}Ag_{0.01}Se$-1.5% SrSe at 823 K (Figure 5c). For BaSe-alloyed samples, a similar value of $\approx 0.62\ Wm^{-1}K^{-1}$ is obtained for $Pb_{0.99}Ag_{0.01}Se$-3% BaSe at 823 K (Figure 5d). The lowest κ_{lat} values for SrSe- and BaSe-alloyed samples decrease by 35% and 33% compared with $0.93\ Wm^{-1}K^{-1}$ for $Pb_{0.99}Ag_{0.01}Se$ at 823 K, respectively.

According to our TEM results, SrSe alloying reduces the solubility of Ag in the PbSe matrix and causes a large amount of Ag-rich nanoprecipitates with a size range of 5–80 nm, which homogeneously distributed in the matrix (Figure 1b). Thus, we suggest the nanoscale Ag-rich precipitates, the off-centered Ag dopants, and the point defect caused by the Sr- or Ba-alloying significantly impeded phonon propagation and contributed to the reduction of κ_{lat}. Despite the slight rise of κ_{lat} at above 823 K, which is likely caused by the bipolar diffusion of increased minority carriers, the contribution of bipolar diffusion is minimal in these SrSe- and BaSe-alloyed samples because of the enlarged band gaps. Although the nanoscale precipitates and point defect usually lead to reduced charge mobility (μ_H), Ag-doped PbSe samples show much higher $\mu_H \approx 280\ cm^2V^{-1}s^{-1}$ compared to $\approx 230\ cm^2V^{-1}s^{-1}$ for Na-doped PbSe standard sample with $n \approx 5.99 \times 10^{19}$.[11b] Moreover, Sr/BaSe alloyed samples show higher μ_H than previous alloyed p-type PbSe-based materials (Figure S11b).[10,11b,13a,15,18]

The temperature-dependent ZT of $Pb_{0.99}Ag_{0.01}Se$-x% SrSe and $Pb_{0.99}Ag_{0.01}Se$-y% BaSe samples is displayed in Figure 6. The SrSe-alloyed samples possess a high peak ZT of ≈ 1.2 at 873 K for $Pb_{0.99}Ag_{0.01}Se$-1.5% SrSe, while the BaSe-alloyed samples show a higher room-temperature ZT of ≈ 0.21 (about four times that of Na-doped PbSe, ≈ 0.05, with $n \approx 3 \times 10^{19}\ cm^{-3}$) for the samples with $y = 4$ and 5. Moreover, the Ag-doped and SrSe- or BaSe-alloyed samples show superior ZT values compared with the state-of-the-art p-type PbSe and Na-doped PbSe compounds over the temperature range of 300–800 K (Figure 6c).[5a,b,11] The greatest benefit is obtained in ZT_{avg} which is crucial in device fabrication. In the range of 400–923 K, the ZT_{avg} is 0.86 for $Pb_{0.99}Ag_{0.01}Se$-1.5% SrSe and ≈ 0.79 for $Pb_{0.99}Ag_{0.01}Se$-3% BaSe. The comparison of ZT_{avg} values with previous p-type PbSe compounds is illustrated in Figure 6d. Noticeably, the value of 0.86 with the theoretical conversion efficiency of $\approx 11.5\%$ in the temperature range of 400–923 K is the highest reported for any p-type PbSe material (Figure 6d).[5a,b,11b]

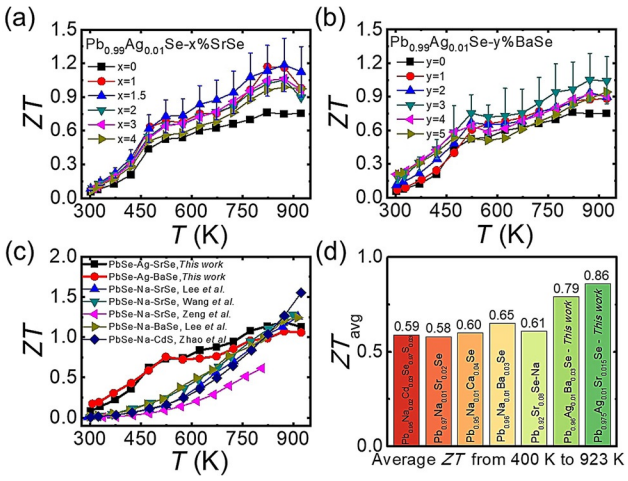

Figure 6. The Figure of merit, *ZT*, as a function of temperature for $Pb_{0.99}Ag_{0.01}Se$-*x*%SrSe (a) and $Pb_{0.99}Ag_{0.01}Se$-*y*%BaSe (b); Comparison of *ZT* values for p-type PbSe-based materials in this study with previously explored p-type PbSe thermoelectric materials (c)[5a,b,11] and comparison of ZT_{avg} values for a temperature gradient of 400 K to 923 K for top performing p-type PbSe-based materials (d).[5a,b,18]

Conclusion

We achieve a substantially improved thermoelectric performance in p-type PbSe-based materials via the use of two independent chemical agents Ag and Sr/Ba which work independently and synergistically to favorably modify the electronic band structure and reduce κ_{lat}. The Ag 4d states make a large contribution to heavy valence band maximum (along Σ) and decreases ΔE_v of PbSe, which cannot be achieved by classical Na and K doping. This leads to the beneficial effect of decreasing the ΔE_v further to ≈ 0.14 eV at 800 K, leading to the significantly enhanced DOS effective mass and Seebeck coefficient. This is the first time a significant modification on the orbital constitution of the top of the heavy hole valence band has been achieved by a metallic dopant that is, Ag. It opens new way to control a challenging part of the electronic structure: heavy hole valence band. Furthermore, Ag-rich nanoscale precipitates, the discordant nature of Ag dopant, and Pb/Sr, Pb/Ba point defects in the PbSe matrix work together to significantly suppress phonon propagation speed and reduce the lattice thermal conductivity to $\approx 0.60\ Wm^{-1}K^{-1}$ at 823 K. By consequence, a record high average ZT_{ave} of ≈ 0.86 is obtained for $Pb_{0.99}Ag_{0.01}Se$-1.5% SrSe, showing the considerable potential of this tellurium-free system for device applications.

Acknowledgements

This work was supported mainly by the Department of Energy, Office of Science Basic Energy Sciences under grant DE-SC0014520, DOE Office of Science (sample preparation, synthesis, XRD, TE measurements, TEM measurements, DFT calculations). ZZL and QY gratefully acknowledge the National Natural Science Foundation of China (61728401). This work also made use of the EPIC facility of Northwestern University's NUANCE Center, which has received support from the Soft and Hybrid Nanotechnology Experimental (SHyNE) Resource (NSF ECCS-1542205); the MRSEC program (NSF DMR-1720139) at the Materials Research Center; the International Institute for Nanotechnology (IIN); the Keck Foundation; the State of Illinois, through the IIN; the Office of Science of the U.S. Department of Energy under Contract No. DE-AC02-06CH11357 and DE-AC02-05CH11231. Access to facilities of high performance computational resources at the Northwestern University is acknowledged. The authors also acknowledge Singapore MOE AcRF Tier 2 under Grant Nos. 2018-T2-1-010, Singapore A*STAR Pharos Program SERC 1527200021 and

1527200022, Singapore A*STAR project A19D9a0096, the support from FACTs of Nanyang Technological University for sample analysis.

Conflict of interest

The authors declare no conflict of interest.

Keywords: band convergence · lead chalcogenides · nanostructuring · silver doping · thermoelectricity

[1] L.-D. Zhao, S.-H. Lo, Y. Zhang, H. Sun, G. Tan, C. Uher, C. Wolverton, V. P. Dravid, M. G. Kanatzidis, *Nature* **2014**, *508*, 373 – 377.

[2] a) K. F. Hsu, S. Loo, F. Guo, W. Chen, J. S. Dyck, C. Uher, T. Hogan, E. K. Polychroniadis, M. G. Kanatzidis, *Science* **2004**, *303*, 818 – 821; b) G. Tan, L.-D. Zhao, M. G. Kanatzidis, *Chem. Rev.* **2016**, *116*, 12123 – 12149; c) T. Zhu, Y. Liu, C. Fu, J. P. Heremans, J. G. Snyder, X. Zhao, *Adv. Mater.* **2017**, *29*, 1605884; d) J. He, T. M. Tritt, *Science* **2017**, *357*, 1369; e) J. R. Sootsman, D. Y. Chung, M. G. Kanatzidis, *Angew. Chem. Int. Ed.* **2009**, *48*, 8616 – 8639; *Angew. Chem.* **2009**, *121*, 8768 – 8792; f) A. J. Minnich, M. S. Dresselhaus, Z. F. Ren, G. Chen, *Energy Environ. Sci.* **2009**, *2*, 466; g) G. J. Snyder, E. S. Toberer, *Nat. Mater.* **2008**, *7*, 105 – 114; h) L.-D. Zhao, C. Chang, G. Tan, M. G. Kanatzidis, *Energy Environ. Sci.* **2016**, *9*, 3044 – 3060; i) W. G. Zeier, A. Zevalkink, Z. M. Gibbs, G. Hautier, M. G. Kanatzidis, G. J. Snyder, *Angew. Chem. Int. Ed.* **2016**, *55*, 6826 – 6841; *Angew. Chem.* **2016**, *128*, 6938 – 6954; j) Z.-Z. Luo, Y. Zhang, C. Zhang, H. T. Tan, Z. Li, A. Abutaha, X.-L. Wu, Q. Xiong, K. A. Khor, K. Hippalgaonkar, J. Xu, H. H. Hng, Q. Yan, *Adv. Energy Mater.* **2017**, *7*, 1601285.

[3] a) Z.-Z. Luo, S. Hao, S. Cai, T. P. Bailey, G. Tan, Y. Luo, I. Spanopoulos, C. Uher, C. Wolverton, V. P. Dravid, Q. Yan, M. G. Kanatzidis, *J. Am. Chem. Soc.* **2019**, *141*, 6403 – 6412; b) X.-L. Shi, J. Zou, Z.-G. Chen, *Chem. Rev.* **2020**, *120*, 7399 – 7515.

[4] a) Z.-Z. Luo, X. Zhang, X. Hua, G. Tan, T. P. Bailey, J. Xu, C. Uher, C. Wolverton, V. P. Dravid, Q. Yan, M. G. Kanatzidis, *Adv. Funct. Mater.* **2018**, *28*, 1801617; b) Z.-Z. Luo, S. Cai, S. Hao, T. P. Bailey, X. Su, I. Spanopoulos, I. Hadar, G. Tan, Y. Luo, J. Xu, C. Uher, C. Wolverton, V. P. Dravid, Q. Yan, M. G. Kanatzidis, *J. Am. Chem. Soc.* **2019**, *141*, 16169 – 16177; c) L. Yang, Z.-G. Chen, M. Hong, L. Wang, D. Kong, L. Huang, G. Han, Y. Zou, M. Dargusch, J. Zou, *Nano Energy* **2017**, *31*, 105 – 112.

[5] a) L.-D. Zhao, S. Hao, S.-H. Lo, C.-I. Wu, X. Zhou, Y. Lee, H. Li, K. Biswas, T. P. Hogan, C. Uher, C. Wolverton, V. P. Dravid, M. G. Kanatzidis, *J. Am. Chem. Soc.* **2013**, *135*, 7364 – 7370; b) H. Wang, Z. M. Gibbs, Y. Takagiwa, G. J. Snyder, *Energy Environ. Sci.* **2014**, *7*, 804 – 811; c) Q. Zhang, F. Cao, W. Liu, K. Lukas, B. Yu, S. Chen, C. Opeil, D. Broido, G. Chen, Z. Ren, *J. Am. Chem. Soc.* **2012**, *134*, 10031 – 10038; d) Y. Liu, L. You, C. Wang, J. Zhang, J. Yang, K. Guo, J. Luo, W. Zhang, *J. Electron. Mater.* **2018**, *47*, 2584 – 2590; e) C. Gayner, K. K. Kar, W. Kim, *Mater. Today Energy* **2018**, *9*, 359 – 376; f) L. C. Chen, P. Q. Chen, W. J. Li, Q. Zhang, V. V. Struzhkin, A. F. Goncharov, Z. Ren, X. J. Chen, *Nat. Mater.* **2019**, *18*, 1321 – 1326; g) L. You, Y. Liu, X. Li, P. Nan, B. Ge, Y. Jiang, P. Luo, S. Pan, Y. Pei, W. Zhang, G. J. Snyder, J. Yang, J. Zhang, J. Luo, *Energy Environ. Sci.* **2018**, *11*, 1848 – 1858; h) M. Hong, Z.-G. Chen, S. Matsumura, J. Zou, *Nano Energy* **2018**, *50*, 785 – 793; i) Z. Chen, B. Ge, W. Li, S. Lin, J. Shen, Y. Chang, R. Hanus, G. J. Snyder, Y. Pei, *Nat. Commun.* **2017**, *8*, 13828; j) Q. Zhang, H. Wang, W. Liu, H. Wang, B. Yu, Q. Zhang, Z. Tian, G. Ni, S. Lee, K. Esfarjani, G. Chen, Z. Ren, *Energy Environ. Sci.* **2012**, *5*, 5246 – 5251; k) C.-F. Wu, T.-R. Wei, J.-F. Li, *APL Mater.* **2016**, *4*, 104801.

[6] Z. Pan, H. Wang, *J. Mater. Chem. A* **2019**, *7*, 12859 – 12868.

[7] Y. Pei, X. Shi, A. LaLonde, H. Wang, L. Chen, G. J. Snyder, *Nature* **2011**, *473*, 66 – 69.

[8] Y. Takagiwa, Y. Pei, G. Pomrehn, G. J. Snyder, *APL Mater.* **2013**, *1*, 011101.

[9] Z.-Z. Luo, S. Hao, X. Zhang, X. Hua, S. Cai, G. Tan, T. P. Bailey, R. Ma, C. Uher, C. Wolverton, V. P. Dravid, Q. Yan, M. G. Kanatzidis, *Energy Environ. Sci.* **2018**, *11*, 3220 – 3230.

[10] G. Tan, S. Hao, S. Cai, T. P. Bailey, Z. Luo, I. Hadar, C. Uher, V. P. Dravid, C. Wolverton, M. G. Kanatzidis, *J. Am. Chem. Soc.* **2019**, *141*, 4480 – 4486.

[11] a) L. Zeng, J. Zhang, L. You, H. Zheng, Y. Liu, L. Ouyang, P. Huang, J. Xing, J. Luo, *J. Alloys Compd.* **2016**, *687*, 765 – 772; b) Y. Lee, S. H. Lo, J. Androulakis, C. I. Wu, L. D. Zhao, D. Y. Chung, T. P. Hogan, V. P. Dravid, M. G. Kanatzidis, *J. Am. Chem. Soc.* **2013**, *135*, 5152 – 5160.

[12] M. Hong, Y. Wang, T. Feng, Q. Sun, S. Xu, S. Matsumura, S. T. Pantelides, J. Zou, Z.-G. Chen, *J. Am. Chem. Soc.* **2019**, *141*, 1742 – 1748.

[13] a) S. Cai, S. Hao, Z.-Z. Luo, X. Li, I. Hadar, T. P. Bailey, X. Hu, C. Uher, Y.-Y. Hu, C. Wolverton, V. P. Dravid, M. G. Kanatzidis, *Energy Environ. Sci.* **2020**, *13*, 200 – 211; b) J. M. Hodges, S. Hao, J. A. Grovogui, X. Zhang, T. P. Bailey, X. Li, Z. Gan, Y. Y. Hu, C. Uher, V. P. Dravid, C. Wolverton, M. G. Kanatzidis, *J. Am. Chem. Soc.* **2018**, *140*, 18115 – 18123; c) L. D. Zhao, H. J. Wu, S. Q. Hao, C. I. Wu, X. Y. Zhou, K. Biswas, J. Q. He, T. P. Hogan, C. Uher, C. Wolverton, V. P. Dravid, M. G. Kanatzidis, *Energy Environ. Sci.* **2013**, *6*, 3346 – 3355; d) G. Tan, F. Shi, S. Hao, L.-D. Zhao, H. Chi, X. Zhang, C. Uher, C. Wolverton, V. P. Dravid, M. G. Kanatzidis, *Nat. Commun.* **2016**, *7*, 12167.

[14] J. M. Skelton, S. C. Parker, A. Togo, I. Tanaka, A. Walsh, *Phys. Rev. B* **2014**, *89*, 205203.

[15] T. J. Slade, T. P. Bailey, J. A. Grovogui, X. Hua, X. Zhang, J. J. Kuo, I. Hadar, G. J. Snyder, C. Wolverton, V. P. Dravid, C. Uher, M. G. Kanatzidis, *Adv. Energy Mater.* **2019**, *9*, 1901377.

[16] H. Wang, Y. Pei, A. D. LaLonde, G. J. Snyder, *Adv. Mater.* **2011**, *23*, 1366 – 1370.

[17] H.-S. Kim, Z. M. Gibbs, Y. Tang, H. Wang, G. J. Snyder, *APL Mater.* **2015**, *3*, 041506.

[18] Q. Lin, S. Tepfer, C. Heideman, C. Mortensen, N. Nguyen, P. Zschack, M. Beekman, D. C. Johnson, *J. Mater. Res.* **2011**, *26*, 1866 – 1871.

Manuscript received: August 28, 2020
Accepted manuscript online: September 14, 2020
Version of record online: October 27, 2020

